Laser Physics Letters

Astro Ltd.

LETTER

# Modulation gain and squeezing by dressed state in hot atomic system

IOP Publishing | Astro Ltd
Laser Physics Letters
Laser Phys. Lett. **16** (2019) 055401 (6pp)
https://doi.org/10.1088/1612-202X/ab11e4

Letter

# Modulation gain and squeezing by dressed state in hot atomic system

**Changbiao Li[1,2], Bingling Gu[1], Da Zhang[1], Wenjie Chen[1], Zan Shen[1], Guangchen Lan[1] and Yanpeng Zhang[1]**

[1] Key Laboratory for Physical Electronics and Devices of the Ministry of Education & Shaanxi Key Lab of Information Photonic Technique, Xi'an Jiaotong University, Xi'an 710049, People's Republic of China
[2] School of Science, Xi'an Jiaotong University, Xi'an 710049, People's Republic of China

E-mail: ypzhang@mail.xjtu.edu.cn

Received 1 December 2018
Accepted for publication 5 March 2019
Published 9 April 2019

**Abstract**

We report that the optical gain and intensity difference squeezing (IDS) of four-wave mixing can be controlled using an external dressing field in a hot rubidium atomic system. The intensity of the parametric amplified four-wave mixing (PA-FWM) signal in the probe and corresponding conjugate channels can be enhanced using the dressed effect, resulting in an increase of the optical gain. So, the IDS in the dressed PA-FWM has a higher degree of −7.1 dB, as compared to that in the PA-FWM of −2.5 dB. This scheme of enhancing the optical gain and the generated IDS requires a simple experimental setup that is mechanically stable. These outcomes can be used in the fabrication of quantum devices and the realization of quantum metrology.

Keywords: intensity difference squeezing, parametric amplified four-wave mixing, gain

(Some figures may appear in colour only in the online journal)

## 1. Introduction

The quantum entanglement state plays an important role in the field of quantum information processing because of its strong correlation and due to the no-cloning theorem. Several interesting works have been experimentally applied in the past few years, such as quantum communication networks [1, 2], quantum computation [3, 4], and telecloning [5–8]. Since the early days of research on squeezed states of light [9], it has been verified that four-wave mixing (FWM) in an atomic vapor can generate non-classical states of light, and an approximately −0.2 dB of squeezing was demonstrated in a rubidium (Rb) vapor [10]. The amount of squeezing from FWM in atomic vapors is limited by the spontaneous emission noise and cannot rival parametric down-conversion systems. Recently, narrow-bandwidth, time-frequency entangled, paired photons with two driving lasers running twin continuous wave modes were generated using electromagnetically induced transparency (EIT) [11] and spontaneous parametric FWM (SP-FWM), which not only possess narrow bandwidths but also automatically match the atomic transitions [12, 13]. Subsequently, a relative noise reduction of −3.5 dB was observed in non-degenerate FWM process based on coherent population trapping in atomic vapors, and then the best squeezing of −8.8 dB was optimized over a large frequency range [15]. Furthermore, the relative intensity squeezing up to 9.2 dB below the standard quantum limit was measured in [16]. The atomic ground state coherence built from this system has successfully suppressed the excess noise that limited earlier atomic vapor-based squeezing generation methods. This system has been used for a number of applications, such as strong, low-frequency, quantum correlated beams [15], quantum entangled imaging [17], and the generation of high-purity, narrow-band, single photons [18]. To increase the degree of intensity difference squeezing (IDS), the technique of cascading more stages of the parametric amplified FWM (PA-FWM) process has been demonstrated. The

 

IDS is enhanced to $(-7.0 \pm 0.1)$ dB from $(-5.5 \pm 0.1)$ dB/$(-4.5 \pm 0.1)$ dB initial squeezing using two cascaded atomic vapor cells [19]. Similarly, enhanced, continuous-variable, squeezed states have also been realized using two cascading PA down-conversion processes with two separate nonlinear crystals [20]. The ultimate enhancement limit that is reachable using additional stages of these cascade setups can be theoretically derived [21].

Enhanced FWM processes due to atomic coherence have been experimentally observed in the atomic system using EIT [22–25]. Since the degree of IDS is mainly determined by the high optical gain realizable in the PA-FWM process, we develop an efficient way to enhance the optical gain in the same atomic medium, so the degree of IDS can be enhanced to $(-8.1 \pm 0.4)$ dB or $(-9.0 \pm 0.4)$ dB from a $(-3.6 \pm 0.4)$ dB initial squeezing [26]. Compared with the case of a single cell, this model has a lower pump power limit and higher gain saturation limit because of the degenerate multi-wave mixing process. This IDS light source may find potential applications in quantum metrology [27, 28], quantum communication [29, 30], and quantum information processing [31].

In this paper, we report that the optical gain and IDS can be controlled by the dressing effect of an extreme field. The dressing effect can enhance the PA-FWM signals in the probe and corresponding conjugate channels, while the absorption of the medium is also increased due to the electromagnetically induced absorption (EIA). There is a competition between the loss and gain of the atomic system, which change with the detuning and the Rabi frequency of the dressing field. Our goal is to find optimized conditions that enhance the IDS.

## 2. Theory and experimental setup

We consider a four-level atomic system as shown in figure 1(a). The four relevant energy levels are $5S_{1/2}$, $F = 2$ ($|0\rangle$), $5S_{1/2}$, $F = 3$ ($|1\rangle$), $5P_{1/2}$ ($|2\rangle$), and $5P_{3/2}$ ($|3\rangle$) in $^{85}$Rb. The three-level 'double-$\Lambda$' type subsystem ($|0\rangle \leftrightarrow |1\rangle \leftrightarrow |2\rangle$) (see figure 1(a)), is used to generate the SP-FWM process. Two laser beams derived from a Ti:sapphire laser and an external cavity diode laser (ECDL) are coupled into the corresponding transitions. With the laser frequency tuned to the $D1$ line transition (795 nm), the strong pump beam $\boldsymbol{E}_1$ (frequency $\omega_1$, wave vector $\mathbf{k}_1$, Rabi frequency $G_1$, and vertical polarization) up to 350 mW is coupled into the cell with the polarizing beam splitting (PBS). The weak probe beam $\boldsymbol{E}_2$ ($\omega_2$, $\mathbf{k}_2$, $G_2$, and horizontal polarization) at approximately 100 $\mu$W propagates in the same direction as $\boldsymbol{E}_1$. An EIT window will be created for the probe field due to the two-photon, Doppler-free configuration in this Doppler-broadened atomic medium. The SP-FWM process involves coupled Stokes channel and anti-Stokes channel, and produces twin photons. Such SP-FWM process with the Hamiltonian can be written as [26]

$$H = \frac{\kappa}{v}\left(\hat{a}^{+}\hat{b}^{+} + \hat{a}\hat{b}\right), \tag{1}$$

where $\hat{a}^{+}(\hat{a})$ is the creation (-annihilation) operator that acts on the electromagnetic excitation of the $\boldsymbol{E}_S$ channel, whereas $\hat{b}^{+}\left(\hat{b}\right)$ acts on the $\boldsymbol{E}_{aS}$ channel. $v$ is the group velocity of light in the nonlinear medium, and $\kappa = \left|\chi^{(3)}\boldsymbol{E}_1\boldsymbol{E}_1\right| = \left|N\mu_{10}^2\rho_{S/aS}^{(3)}/\hbar\varepsilon_0 G_{S/aS}\right|$ is the pumping parameter of the SP-FWM, which depends on the nonlinearity $\chi^{(3)}$ and the pump-field amplitude. $\varpi_S$ and $\varpi_{aS}$ is the central frequencies of generated Stokes and anti-Stokes signals. With the detuning of $\boldsymbol{E}_1$ tuned far away from the resonance, the FWM process will occur in the subsystem, which can generate the Stokes field ($\boldsymbol{E}_S$) and anti-Stoke field ($\boldsymbol{E}_{aS}$) (satisfying the phase-match condition (PMC) $2\mathbf{k}_1 = \mathbf{k}_S + \mathbf{k}_{aS}$). Under the dipole and rotating-wave approximation, the Hamiltonian for this system can be described as: $H_{\rm int} = -\hbar\left[\Delta_1 |2\rangle\langle 2| + (-\Delta_1 + \Delta_1')|1\rangle\langle 1|\right] - \hbar\left(G_1|2\rangle\langle 0| + G_1|2\rangle\langle 1|\right)$, where $G_i = \mu_{ij}E_i/\hbar$ is the Rabi frequency of field $\boldsymbol{E}_i$ with the electric dipole matrix elements $\mu_{ij}$. Such an SP-FWM can be described using a perturbative chain: $\rho_{11}^{(0)} \xrightarrow{\omega_1} \rho_{21}^{(1)} \xrightarrow{\omega_{aS}} \rho_{01}^{(2)} \xrightarrow{\omega_1} \rho_{21(S)}^{(3)}$ ($\boldsymbol{E}_S$) and $\rho_{00}^{(0)} \xrightarrow{\omega_1} \rho_{20}^{(1)} \xrightarrow{\omega_S} \rho_{10}^{(2)} \xrightarrow{\omega_1} \rho_{20(aS)}^{(3)}$ ($\boldsymbol{E}_{aS}$) [32, 33]. The evolution of the variables in the interaction representation is governed by the master equation, $\partial\rho/\partial t = -i\left[H_{\rm int}, \rho\right]/\hbar + \left(\partial\rho/\partial t\right)_{inc}$, where the first term results from coherent interactions and the second term represents damping due to decays with or without emission, dephasing, and other irreversible process. Under the steady-state approximations, the intensities of the Stokes field ($\boldsymbol{E}_S$) and anti-Stoke field ($\boldsymbol{E}_{aS}$) can be described by the density matrix elements $\rho_{21(S)}^{(3)}$ and $\rho_{20(aS)}^{(3)}$, which are given by

$$\rho_{21(S)}^{(3)} = -iG_{aS}^{*}G_1^2/\left(d_{21}d_{01}d_{21}'\right) \tag{2a}$$

$$\rho_{20(aS)}^{(3)} = -iG_S^{*}G_1^2/\left(d_{20}d_{10}d_{20}'\right) \tag{2b}$$

where $d_{20} = \Gamma_{20} + i\Delta_1$, $d_{10} = \Gamma_{10} + i(\Delta_1 - \Delta_S)$, $d_{20}' = \Gamma_{20} + i(\Delta_1 - \Delta_S + \Delta_1')$, $d_{21} = \Gamma_{21} + i\Delta_1'$, $d_{01} = \Gamma_{01} + i(\Delta_1' - \Delta_{aS})$, and $d_{21}' = \Gamma_{21} + i(\Delta_1 - \Delta_{aS} + \Delta_1')$ with $\Delta_S$ and $\Delta_{aS}$ representing the frequency detuning of the $\boldsymbol{E}_S$ and $\boldsymbol{E}_{aS}$ signals. The $\Delta_1'$ and $\Delta_1$ are the frequency detuning of the $\boldsymbol{E}_1$ field from the transitions $|1\rangle \rightarrow |2\rangle$ and $|0\rangle \rightarrow |2\rangle$, respectively, and $\Gamma_{ij} = (\Gamma_i + \Gamma_j)/2$ is the de-coherence rate between $|i\rangle$ and $|j\rangle$.

Moreover, the probe field and vacuum field (i.e. $|\alpha, 0\rangle$) are injected into the Stokes and anti-Stokes ports of the SP-FWM process, respectively. Then, the entire process can be viewed as a PA-FWM process. Therefore, the optical gain is given $\boldsymbol{G}_F = \cosh^2(\kappa L)$, where $\kappa \propto \rho_{S/aS}^{(3)}$. Finally, IDS between $\boldsymbol{E}_S$ and $\boldsymbol{E}_{aS}$ is $S_q = -\mathrm{Log}_{10}\left(2G_F - 1\right)$ [24, 25]. Considering the loss in probe and conjugate fields, IDS can be modified as [34]

$$S_q = 10\mathrm{Log}\left[1 + \frac{2\left(G_F - 1\right)\left[G_F(\eta_a - \eta_b)^2 - \eta_b^2\right]}{G_F\eta_a + \left(G_F - 1\right)\eta_b}\right], \tag{3}$$

where $\eta_a$ and $\eta_b$ are the fraction of the probe and conjugate beams transmitted/detected.

In an atomic coherence system, the optical gain $G_F$ can be modified using multiple parameters. We turn to the case with the strong coupling field $\boldsymbol{E}_3$ ($\omega_3$, $\mathbf{k}_3$, and $G_3$) coupling to the

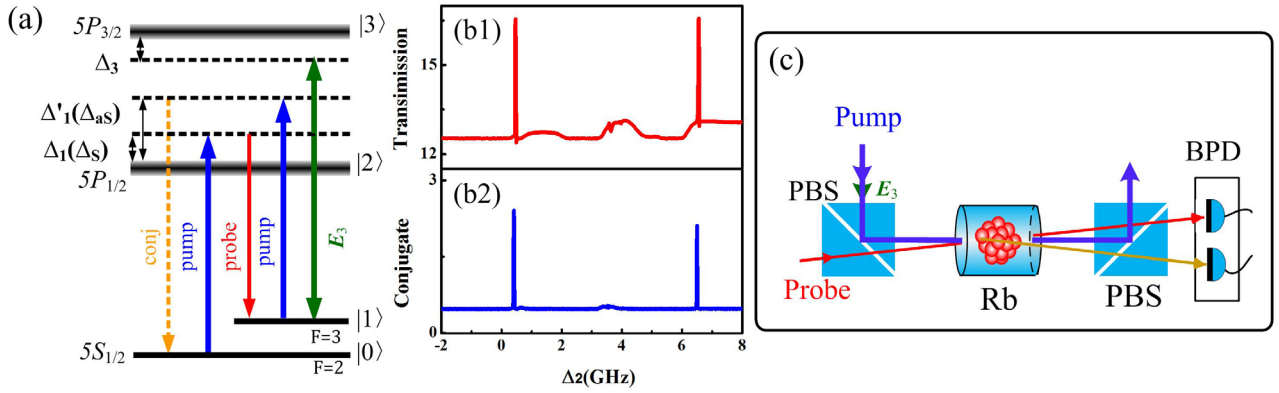


**Figure 1.** (a) Energy-level diagram. (b1) and (b2) Measured probe transmission signal and corresponding conjugate signal versus the probe frequency detuning $\Delta_2$. (c) Experimental setup scheme showing the PBS (polarizing beam splitter) and BPD (balanced homodyne photodiode detector).

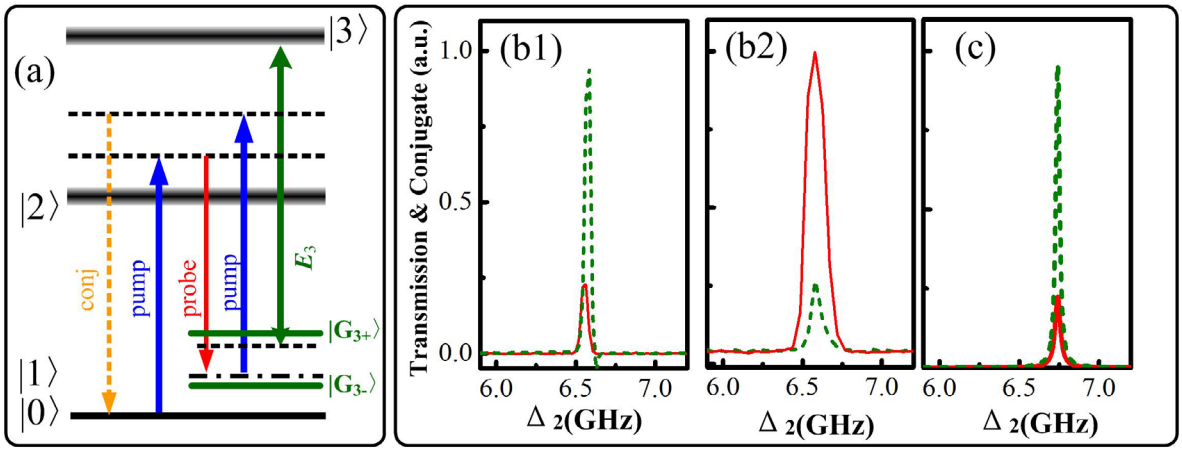


**Figure 2.** (a) The dressed-state picture for the enhancement of the PA-FWM process. (b1) and (b2) Measured probe transmission signal ($\boldsymbol{E}_S$) and the corresponding conjugate signal ($\boldsymbol{E}_{aS}$) versus the probe detuning, respectively, for a pump detuning as indicated by the arrow. The solid lines indicate $\boldsymbol{E}_3$ is off, and the dashed lines indicate $\boldsymbol{E}_3$ is on with $\Delta_3 = 0.43$ GHz. (c) The theoretical plots using experimental parameters. Panels (b2) and (c) share the same intensity (vertical) scale as (b1).

transition $|1\rangle \leftrightarrow |3\rangle$. Taking into account the dressing effect of $\boldsymbol{E}_3$, equations (2*a*) and (2*b*) can be rewritten as [32, 35]:

$$\rho'^{(3)}_{21(s)} = -iG_1^2 G_{as}/d_{21}d_{01D}d'_{21}, \tag{4a}$$

$$\rho'^{(3)}_{20(as)} = -iG_1^2 G_s/d_{20}d_{10D}d'_{20}, \tag{4b}$$

where $d_{01D} = d_{01} + G_3^2/d_{31}$, $d_{31} = \Gamma_{31} + i(\Delta'_1 - \Delta_{as} + \Delta_3)$, $d_{10D} = d_{10} + G_3^2/d_{13}$, and $d_{13} = \Gamma_{13} + i(\Delta_1 - \Delta_s - \Delta_3)$ with $\Delta_3$ defined as the frequency detuning of the $\boldsymbol{E}_3$ field from the transition $|1\rangle \rightarrow |3\rangle$. The dressing field couples the transition $|1\rangle \leftrightarrow |3\rangle$ and creates the dressed states $|G_{3\pm}\rangle$ (figure 2(a)). Therefore, the PA-FWM signal for a large detuning is extremely small when $G_3 = 0$, and the strong dressing field can cause resonant excitations for one of the dressed states if the condition $(\Delta_1 - \Delta_S - \Delta_3 \pm \Delta_{G_3} = 0)$ is satisfied, where $\Delta_{G_3}$ is the splitting level relative to the original position of the state $|1\rangle$ by the dressing field $\boldsymbol{E}_3$. So, the PA-FWM signal is strongly enhanced, and results in the enhancement of the optical gain $G_F$. On the other hand, the absorption of

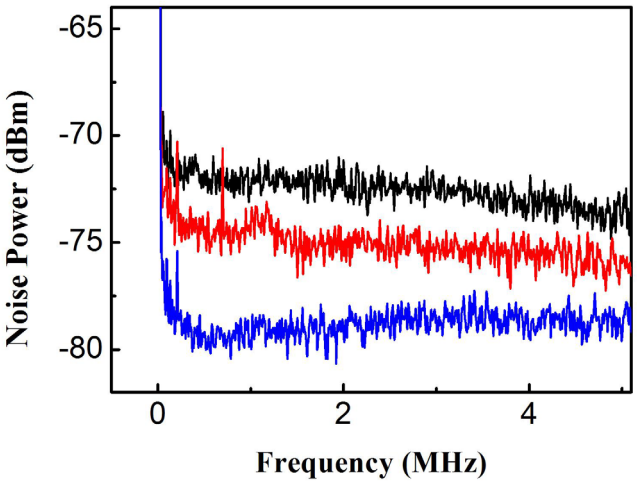


**Figure 3.** Relative intensity noise levels versus the spectrum analyzer frequency. SNL (top curve), PA-FWM (middle curve), and dressed PA-FWM when field $\boldsymbol{E}_3$ is applied (bottom curve). The background noise is subtracted from all of the traces.

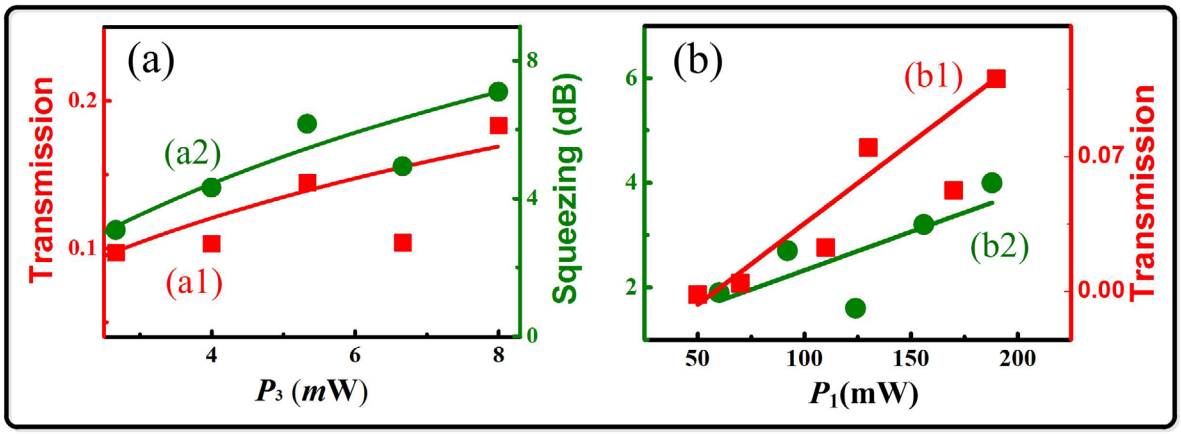


**Figure 4.** (a) Relationship of the probe transmission (a1), and IDS (a2) of the dressed PA-FWM versus the dressing power ($\boldsymbol{P}_3$), $\boldsymbol{P}_1 = 350$ mW. (b) Relationship of the probe transmission (b1) and IDS (b2) of the dressed PA-FWM versus the pump power ($\boldsymbol{P}_1$), $\boldsymbol{P}_3 = 8$ mW. Solid curves are the theoretical predictions.

medium is also increased due to the EIA generated by the external dressing fields. Fortunately, the overall effect of the dressing field shows the gain is enhanced in the conditions of $(\Delta_1 - \Delta_S - \Delta_3 \pm \Delta_{G_3} = 0)$. We define the optical gain coefficient related to the matrix element $\rho'_{(S/aS)}$ as the dressed optical gain coefficient $\boldsymbol{G}_{dF} = \cosh^2(\kappa L)$, where $\kappa \propto \rho'^{(3)}_{S/aS}$. Thus, both the nonlinear coefficient $\kappa$ and $\boldsymbol{G}_{dF}$ increase. It can be concluded that the degree of squeezing can be increased when the enhancement condition of the PA-FWM is satisfied. Therefore, the IDS between the $\boldsymbol{E}_S$ and $\boldsymbol{E}_{aS}$ is $S_q = 10\mathrm{Log}\left[1 + \frac{2(G_{dF}-1)\left[G_{dF}(\eta_a-\eta_b)^2-\eta_b^2\right]}{G_{dF}\eta_a+(G_{dF}-1)\eta_b}\right]$. In previous literature [14, 19], the optimized nonlinear gain is mainly regulated by the single photon detuning and two photon detuning, which is different from our theoretical model. In our model, two photon detuning is also a tunable parameter, but it is strongly dependent on the Rabi frequency of dressing field. In addition, the introduction of the external dressing field enhances the nonlinear coefficient of the system, which has been proved theoretically [36]. On the other hand, the dressed field will cause the population transfer effect which means that the nonlinear gain will further increased [26]. That is, our system has a higher gain saturation limit than the previous model.

We heat a natural rubidium vapor cell to 130 °C and use a Ti:sapphire laser with a power of up to 350 mW to generate the pump field $\boldsymbol{E}_1$ and an external cavity diode laser (ECDL) to provide the probe field (0.2 mW) in the dressed gain experiment. In the IDS experiment, however, we split the pump light from the Ti:sapphire laser with a PBS into two parts. We let one beam pass through an acousto-optic modulator (AOM) twice. After this process, this beam is tuned to 3.04 GHz to the red of the pump field and acts as the probe field to couple with the other pump light. The weak probe beam $\boldsymbol{E}_2$ propagates in the same direction as $\boldsymbol{E}_1$ with an angle of 0.26°. The dressing field $\boldsymbol{E}_3$ generated by another ECDL propagates in the same direction as $\boldsymbol{E}_1$. The spatial beam trajectories are shown in figure 1(c). Then, the output probe and the conjugate beams are detected with two balanced homodyne photodiode detector. Finally, we use a radio frequency spectrum analyzer (SA) with a resolution bandwidth (RBW) of 300 kHz and a video bandwidth (VBW) of 10 kHz to accept the difference between the two signals, which shows the relative intensity noise power. The generated signals ($\boldsymbol{E}_S$ and $\boldsymbol{E}_{aS}$) are detected with the branch of a balanced and amplified photodetector with a transimpedance gain of $10^5$ V A$^{-1}$ and 91% quantum efficiency. Figures 1(b1) and (b2) show the probe transmission signal and corresponding conjugate signal, respectively, versus the probe frequency detuning $\Delta_2$ at $\Delta_1 = 0.98$ GHz [22, 26].

## 3. Results and discussion

The solid lines in figures 2(b1) and (b2) show the PA-FWM signals in the probe and the corresponding conjugate channels in the double-$\Lambda$ $^{85}$Rb atomic system by scanning the probe field $\boldsymbol{E}_2$ and with the $\boldsymbol{E}_3$ off [26]. When $\boldsymbol{E}_3$ is turned on, the intensity of the PA-FWM signal increases in comparison with the pure PA-FWM signals. This is because the dressing field $\boldsymbol{E}_3$ couples the transition $|3\rangle$ to $|1\rangle$ and creates the dressed states $|G_{3\pm}\rangle$ (figure 2(a)). Since this increases the detuning of the two photons, the enhancement condition $(\Delta_1 - \Delta_S - \Delta_3 \pm \Delta_{G_3} = 0)$ is satisfied. Namely, detuning the two photons meets the bright-state condition, where $\Delta_{G_3}$ is the splitting level (by the dressing field $\boldsymbol{E}_3$) relative to the original position of the state $|1\rangle$. Therefore, the PA-FWM is greatly enhanced, as shown by the dashed line in figure 2(b1). The corresponding PA-FWM signal in the conjugate channel increases, as shown by the dashed line in figure 2(b2). The optical gain is enhanced from ~1.5 (figure 2(b2)) to ~8 (figure 2(b1)) due to the dressed effect. Figure 2(c) presents the theoretical predictions, which agree well with the experimental results.

Then, we investigate the relative intensity noise level between the probe and conjugate channel signals. Firstly, one of the two pump beams from the Ti:sapphire laser passes through the AOM twice and acts as a probe field. The beam out of the AOM is injected into the probe channel. We calibrate the shot noise limit (SNL) using a coherent beam whose power is equal to the total power on our photodiodes. Secondly, we split

this beam 50/50 and direct them into separate photodiodes to record the noise power of the differences. All these noise power spectra are normalized to the corresponding SNL, as shown in the top curve of figure 3. From the middle and bottom curves in figure 3, we find that the IDS of the PA-FWM signal is −2.5 dB, which is below the normalized SNL. When $\boldsymbol{E}_3$ is on, the IDS of the dressed PA-FWM (bottom curve in figure 3) is −7.1 dB, which proves that the degree of squeezing is apparently enhanced by the dressed optical gain $G_{dF}$. This is because the optical gain of the PA-FWM increases from ~1.5 to ~8 due to the dressed effect, as mentioned above. From the relation $S_q = 10\mathrm{Log}\left[1 - 2\left(G_{dF} - 1\right)\eta_b / \left(2G_{dF} - 1\right)\right] \quad (\eta_a = \eta_b)$, the IDS increases as the PA-FWM signal is enhanced and the absorption is decreased. So, the measured IDS of the dressed PA-FWM (bottom curve in figure 3) is up to −7.1 dB, which is much larger than that of the pure PA-FWM at −2.5 dB (middle curve in figure 3). As well known to all, the relative noise reduction will decrease rapidly with the increase of loss. In our optical configuration, the optical loss is about 3%, resulting in a total detection efficiency of 0.88; the uncertainty is estimated at 1 standard. In addition, the population transfer effect is considered in our model [26], which further increases the nonlinear gain and makes the squeezing larger.

Furthermore, we examine the probe transmission and the squeezing of the PA-FWM and dressed PA-FWM by increasing the dressing power. Figure 4(a1) shows the dressed Stokes signals versus the dressing power. The probe transmission increases with the increase of the dressing power, which means that the dressing field $\boldsymbol{E}_3$ significantly enhances the PA-FWM signal. Next, we measure the intensity of the probe transmission signal versus the dressing power. As the power of the dressing field $\boldsymbol{E}_3$ increases, the degree of IDS increases linearly. This is because the $\boldsymbol{E}_3$ field causes two effects: the dressing effect and EIA. The induced EIA will increase the absorption of the medium, but it will greatly increase the nonlinear gain under the two-photon resonance condition. The power also increases the optical gain $G_{dF}$. Meanwhile, we also verify that the relative $Sq_{dF}$ of the dressed PA-FWM signals increases with the increase of the pump power (figure 4(b)). This rule is the same as seen in previous research [23].

## 4. Conclusions

In summary, we have observed an IDS of the PA-FWM processes in a hot Rb vapor. Compared with the pure PA-FWM process, the relative IDS is significantly enhanced to −7.1 gain. Meanwhile, we observe that the relative IDS in the dressed PA-FWM process could be controlled via changing the dressing power. In the quantum enhanced nonlinear interferometer, the sensitivity is proportional to the squeezing of FWM. On the other hand, the entangled state with higher squeezing in continuous variable regime can better resist environmental noise. Compared with previous model our system has a higher gain saturation limit [36]. Such results find potential applications in quantum imaging [37, 38], quantum communication [39] and quantum metrology [28].

## Acknowledgment

This work was supported by National Key R&D Program of China (2017YFA0303703), NSFCs (11474228), China Postdoctoral Science Foundation (2016M590935), NSF of Shaanxi Province (2016JM6029).

## References

[1] Caruso F, Huelga S F and Plenio M B 2010 Noise-enhanced classical and quantum capacities in communication networks *Phys. Rev. Lett.* **105** 190501
[2] Lu C Y, Yang T and Pan J W 2009 Experimental multiparticle entanglement swapping for quantum networking *Phys. Rev. Lett.* **103** 020501
[3] Opatrný T 2017 Quasicontinuous-variable quantum computation with collective spins in multipath interferometers *Phys. Rev. Lett.* **109** 010502
[4] Kyaw T H, Li Y and Kwek L C 2014 Measurement-based quantum computation on two-body interacting qubits with adiabatic evolution *Phys. Rev. Lett.* **113** 180501
[5] Chiuri A, Greganti C, Paternostro M, Vallone G and Mataloni P 2012 Experimental quantum networking protocols via four-qubit hyperentangled Dicke states *Phys. Rev. Lett.* **109** 173604
[6] Zhao Z, Zhang A N, Zhou X Q, Chen Y A, Lu C Y, Karlsson A and Pan J W 2005 Experimental realization of optimal asymmetric cloning and telecloning via partial teleportation *Phys. Rev. Lett.* **95** 030502
[7] Van L P and Braunstein S L 2001 Telecloning of continuous quantum variables *Phys. Rev. Lett.* **87** 247901
[8] Koike S, Takahashi H, Yonezawa H, Takei N, Braunstein S L, Aoki T and Furusawa A 2006 Demonstration of quantum telecloning of optical coherent states *Phys. Rev. Lett.* **96** 060504
[9] Slusher R E, Hollberg L W, Yurke B, Mertz J C and Valley J F 1985 Observation of squeezed states generated by four-wave mixing in an optical cavity *Phys. Rev. Lett.* **55** 2409
[10] van der Wal C H, Eisaman M D, André A, Walsworth R L, Phillips D F, Zibrov A S and Lukin M D 2003 *Science* **301** 196
[11] Harris S E 1997 Electromagnetically induced transparency *Phys. Today* **50** 36
[12] Balic V, Braje D A, Kolchin P, Yin G Y and Harris S E 2005 Generation of paired photons with controllable waveforms *Phys. Rev. Lett.* **94** 183601
[13] Kolchin P, Du S, Belthangady C, Yin G Y and Harris S E 2006 Generation of narrow-bandwidth paired photons: use of a single driving laser *Phys. Rev. Lett.* **97** 113602
[14] McCormick C F, Boyer V, Arimondo E and Lett P D 2007 Strong relative intensity squeezing by four-wave mixing in rubidium vapor *Opt. Lett.* **32** 178
[15] McCormick C F, Marino A M, Boyer V and Lett P D 2008 Stong low-frequency quantum correlations from a four-wave mixing amplifier *Phys. Rev.* A **78** 043816
[16] Glorieux Q, Guidoni L, Guibal S, Likforman J and Coudreau T 2011 Quantum correlations by four-wave mixing in an atomic vapor in a nonamplifying regime: quantum beam splitter for photons *Phys. Rev.* A **84** 053826
[17] Boyer V, Marino A M, Pooser R C and Lett P D 2008 Entangled images from four-wave mixing *Science* **321** 544
[18] MacRae A, Brannan T, Achal R and Lvovsky A I 2012 Tomography of a high-purity narrowband photon from a transient atomic collective excitation *Phys. Rev. Lett.* **109** 033601

[19] Qin Z Z, Cao L M, Wang H L, Marino A M, Zhang W P and Jing J T 2014 Experimental generation of multiple quantum correlated beams from hot rubidium vapor *Phys. Rev. Lett.* **113** 023602
[20] Jia X, Yan Z, Duan Z, Su X, Wang H, Xie C and Peng K 2012 Experimental realization of three-color entanglement at optical fiber communication and atomic storage wavelengths *Phys. Rev. Lett.* **109** 253604
[21] Wang D, Zhang Y and Xiao M 2013 Experimental realization of three-color entanglement at optical fiber communication and atomic storage wavelengths *Phys. Rev.* A **87** 023834
[22] Zhang Y, Khadka U, Anderson B and Xiao M 2009 Temporal and spatial interference between four-wave mixing and six-wave mixing channels *Phys. Rev. Lett.* **102** 013601
[23] Kang H, Hernandez G and Zhu Y 2004 Slow-light six-wave mixing at low light intensities *Phys. Rev. Lett.* **93** 073601
[24] Sevincli S, Henkel N, Ates C and Pohl T 2011 *Phys. Rev. Lett.* **107** 153001
[25] Fleischhauer M, Imamoglu A and Marangos J P 2005 Nonlocal nonlinear optics in cold Rydberg gases *Rev. Mod. Phys.* **77** 633
[26] Zhang D, Li C B, Zhang Z Y, Zhang Y Q, Zhang Y P and Xiao M 2017 Enhanced intensity-difference squeezing via energy-level modulations in hot atomic media *Phys. Rev.* A **96** 043847
[27] Napolitano M, Koschorreck M, Dubost B, Behbood N, Sewell R J and Mitchell M W 2011 Interaction-based quantum metrology showing scaling beyond the Heisenberg limit *Nature* **471** 486
[28] Hudelist F, Kong J, Liu C, Jing J, Ou Z Y and Zhang W 2014 Quantum metrology with parametric amplifier-based photon correlation interferometers *Nat. Commun.* **5** 3049
[29] Davidovich L 1996 Sub-Poissonian processes in quantum optics *Rev. Mod. Phys.* **68** 127
[30] Weedbrook C, Pirandola S, García-Patrón R, Cerf N J, Ralph T C, Shapiro J H and Lloyd S 2012 Gaussian quantum information *Rev. Mod. Phys.* **84** 621
[31] Lvovsky A I and Raymer M G 2009 Continuous-variable optical quantum-state tomography *Rev. Mod. Phys.* **81** 299
[32] Zhang Y P, Brown A W and Xiao M 2007 Opening four-wave mixing and six-wave mixing channels via dual electromagnetically induced transparency windows *Phys. Rev. Lett.* **99** 123603
[33] Zuo Z C, Sun J, Liu X, Jiang Q, Fu G S, Wu L A and Fu P M 2006 Generalized $n$-photon resonant $2n$-wave mixing in an $(n-1)$-level system with phase-conjugate geometry *Phys. Rev. Lett.* **97** 193904
[34] Jasperse M, Turner L D and Scholten R E 2011 Relative intensity squeezing by four-wave mixing with loss: an analytic model and experimental diagnostic *Opt. Express* **19** 3765–74
[35] Nie Z Q, Zheng H B, Li P Z, Yang Y M, Zhang Y P and Xiao M 2008 Interacting multi-wave mixing in a five-level atomic system *Phys. Rev.* A **77** 063829
[36] Chen H X, Qin M Z, Zhang Y Q, Zhang X, Wen F, Wen J M and Zhang Y P 2014 Parametric amplification of dressed multi-wave mixing in an atomic ensemble *Laser Phys. Lett.* **11** 045201
[37] Pooser R C and Lawrie B J 2016 Plasmonic trace sensing below the photon shot noise limit *ACS Photon.* **3** 8
[38] Pooser R C and Lawrie B 2015 Ultrasensitive measurement of microcantilever displacement below the shot-noise limit *Optica* **2** 393
[39] Zhou Y Y, Yu J, Yan Z H, Jia X J, Zhang J, Xie C D and Peng K C 2018 Quantum secret sharing among four players using multipartite bound entanglement of an optical field *Phys. Rev. Lett.* **121** 150502